


1 Plasmonic Nanoantenna Arrays as Efficient Etendue Reducers for 2 Optical Detection

3 Shaojun Wang,^{*,†} Quynh Le-Van,[†] Thibault Peyronel,[‡] Mohammad Ramezani,[†] Niels Van Hoof,[†]
4 Tobias G. Tiecke,[‡] and Jaime Gomez Rivas^{*,†,§}

5 [†]Dutch Institute for Fundamental Energy Research, P.O. Box 6336, 5600 HH Eindhoven, The Netherlands

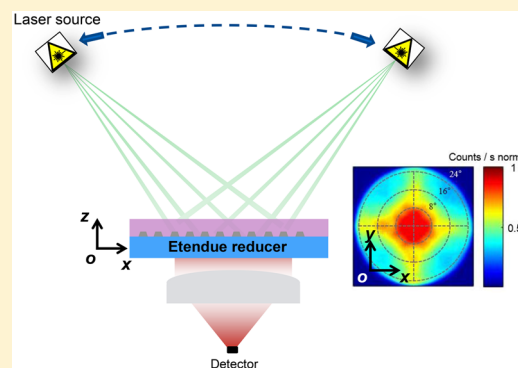
6 [‡]Facebook Inc., Connectivity Lab, 1 Hacker Way, Menlo Park, California 94025, United States

7 [§]Department of Applied Physics, Eindhoven University of Technology, P.O. Box 513, 5600 MB Eindhoven, The Netherlands

8  Supporting Information

9 **ABSTRACT:** Optical detectors require the efficient collection of incident
10 light onto a photodetector. Refractive or reflective optics are commonly
11 used to increase the collected power. However, in the absence of losses,
12 such optics conserve etendue and therefore pose a limit on the field of view
13 and the active area of the detector. A promising method to overcome this
14 limitation is to use an intermediate layer of fluorescent material that
15 omnidirectionally absorbs the incident light and preferentially emits toward
16 the photodetector. We demonstrate here that plasmonic nanoantenna
17 phased arrays are a promising platform to improve the emission efficiency
18 of thin luminescent layers and provide an efficient method to reduce optical
19 etendue. In particular, we show an almost constant optical absorption of the
20 luminescent layer on top of the array with the angle of incidence and a
21 strong beamed emission in small solid angles in the forward direction.
22 These results pave the way for novel optical communication detectors
23 incorporating nanofabricated plasmonic materials as optical etendue reducers.

24 **KEYWORDS:** free-space optical communication, plasmonics, surface lattice resonances, directional emission, fluorescence materials



25 **O**ptical communication applications often require the
26 concentration of light onto a photodetector to magnify
27 the received signal. Using refractive or reflective optics allows
28 for the concentration of light, however, it typically comes at the
29 expense of a reduced field of view because the etendue, that is,
30 the product of the area and field of view, is conserved in the
31 absence of losses. Luminescent materials can act as etendue
32 reducers to concentrate energy onto a photodetector and have
33 been used for solar concentrators,¹ high-energy particle
34 detection,² and recently for free-space optical communications
35 (FSOC).³

36 Desirable characteristics of a photodetector for FSOC
37 include a large bandwidth, a large area and a large field of
38 view to allow for high data rate in the presence of multimode
39 beams with large spatial extent. However, only two of the above
40 characteristics can be matched simultaneously with traditional
41 solid-state detectors. Large area detectors have a slow response
42 time and focusing optics minimize the field of view by
43 conservation of etendue. The etendue can be effectively
44 reduced by using a fluorescent material as an intermediate
45 light conversion layer before detection.³ In this process the
46 laser beam carrying the information is absorbed with near unity
47 efficiency over a wide angle of incidence and is preferentially re-
48 emitted in the direction of the photodetector. In this approach,
49 the spontaneous decay rate of the photoluminescent material

should be as fast as possible for large bandwidth optical 50
communication and the conversion of the incident light and 51
collection efficiency of the emission as high as possible. 52

In this work, we demonstrate a novel geometry where 53
luminescent materials, comprised of fluorescent dye molecules 54
near metallic nanoparticle arrays, achieve light conversion from 55
an incident laser beam over a large field of view and an emission 56
in a small solid angle toward a semiconductor photodetector. 57
This process reduces the etendue of the light field and, when 58
combined with a conventional lens focusing the directionally 59
emitted light, results in a photodetector with an effective large 60
area and a response time set by the decay rate of the fluorescent 61
dye, which can be significantly faster than a semiconductor 62
detector of the same size. Metallic nanoparticles supporting 63
localized surface plasmon resonances (LSPRs), that is, coherent 64
oscillations of the free electrons in the nanoparticle driven by 65
an electromagnetic field, have emerged in recent years as 66
interesting structures to control the emission properties of 67
quantum emitters in their close proximity.^{4,5} This characteristic 68
has led to the description of these structures as optical 69
nanoantennas.⁶ Antenna phased arrays are designed to beam 70
electromagnetic waves in certain directions by controlling the 71

Received: March 6, 2018

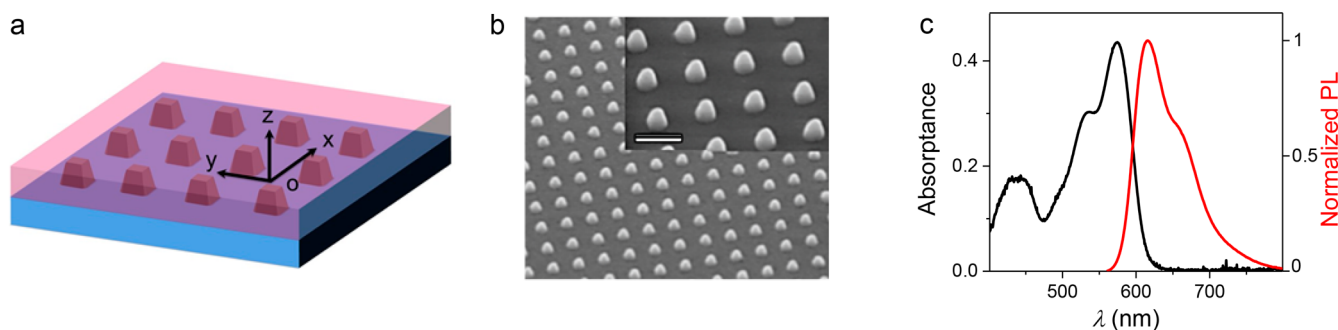


Figure 1. (a) Schematic representation of the sample. From bottom to top: fused silica substrate, Al nanoparticle array and polymer layer containing dye molecules. (b) Side view scanning electron microscope image of the Al nanoparticle array. The scale bar in the inset represents 400 nm. (c) Absorbance (black curve, left axis) and normalized photoluminescence (red curve, right axis) spectrum of a 700 nm thick, 8.5 wt % Lumogen red dye layer.

72 phase difference and interference of the waves radiated by
73 different antennas. Similarly, periodic arrays of metallic
74 nanoparticles constitute the analogue of passive antenna arrays
75 in which the radiation from emitters in their proximity is
76 beamed in defined directions due to scattering of this emission
77 with the periodic structure and interference.^{7–16} Also, lasing
78 from nanoparticles arrays has been reported,^{17–19} and
79 described in terms of cavity modes resulting from the coupling
80 of LSPRs.¹⁸ The emission from these structures can be
81 explained by considering the decay of the emitters into the
82 modes supported by the structure and the radiation of these
83 modes into the far-field.

84 A periodic array of nanoparticles covered with a layer of
85 emitters can support two different types of modes besides
86 LSPRs, called surface lattice resonances (SLRs) and quasi-
87 guided modes. SLRs are the result of the enhanced radiative
88 coupling of LSPRs by the so-called Rayleigh anomalies (RAs),
89 that is, diffracted orders in the plane of the array.²⁰ For quasi-
90 guided modes, the enhancement in the radiative coupling of
91 LSPRs is provided by guided modes in the layer of emitters.^{21,22}
92 In both cases, the dispersion of the modes and the directional
93 outcoupling of the emission is mainly dictated by the
94 periodicity of the array and the polarizability of the constituent
95 nanoparticles. By designing arrays in which the emission of dye
96 molecules is preferential in the direction perpendicular to the
97 surface, we demonstrate that these arrays provide a large
98 improvement in directionality over a bare layer of molecules
99 and constitute a step forward toward a passive etendue reducer.
100 The combination of nanoantenna arrays and dye molecules
101 allows the capture of photons over a large area and field of view,
102 and the re-emission as a collimated beam, which can be
103 subsequently focused onto a small area photodiode.

104 ■ SAMPLE DESCRIPTION AND EMISSION OF DYE 105 LAYERS

106 **Figure 1a** displays a schematic representation of the
107 investigated plasmonic nanoantenna array. The sample consists
108 of a square array of aluminum (Al) nanoparticles with a lattice
109 constant $a = 410$ nm. The shape of the individual nanoparticles
110 is a tapered nanopyramid with a height of 150 nm and a
111 diameter of 80 nm at the top and 140 nm at the base. The
112 nanoantenna array, with a size of 3×3 mm², was fabricated
113 onto a fused silica substrate by substrate conformal nano-
114 imprint lithography (SCIL) followed by reactive ion etching
115 (RIE) of the aluminum.²³ SCIL is based on a flexible rubber
116 stamp, which replicates a pattern containing nanostructures

117 onto a sol–gel that can be further processed. This process can
118 be scaled to large area (wafer size), enabling industrial
119 applications of nanostructured surfaces.²⁴ Each nanoparticle is
120 coated by a thin layer of native oxide (Al₂O₃) that protects it
121 from further oxidation. A scanning electron microscope (SEM)
122 image of the nanoparticle array is shown in **Figure 1b**. A 700
123 nm thick polystyrene layer containing photostable dye
124 molecules (Lumogen red F305, BASF) with a weight percent
125 concentration of 8.5 wt % is deposited on top of the array by
126 spin coating. In what follows, we call this the dye layer. The
127 refractive index of such a dye layer ($n_{\text{dye}} = 1.61$) is larger than
128 that of the substrate beneath ($n_{\text{substrate}} = 1.46$) and the air on
129 top ($n_{\text{air}} = 1$), which renders this layer a planar waveguide. The
130 absorbance and normalized fluorescence spectra of the dye
131 layer are displayed in **Figure 1c**. There are three main
132 absorption peaks at 450, 533, and 575 nm, respectively,
133 corresponding to different energy levels of vibronic transitions
134 in the dye molecules. The emission maximum of the dye layer
135 is at a wavelength of 620 nm.

To ensure that the Al nanoantenna array is coated with the
136 optimum concentration of dye molecules, we explored its
137 ability to efficiently reduce etendue.³ We define a figure of
138 merit (F) characterizing the etendue reduction, i.e. the
139 efficiency with which the luminescent slab absorb photons
140 and remit them in the forward direction in a reduced solid
141 angle, as
142

$$F(\Omega_0) = \frac{4\pi}{\Omega_0} \cdot \frac{\int_0^{\Omega_0} P_{\text{out}}(\lambda_{\text{out}}, \Omega) \cdot d\Omega}{P_{\text{in}}(\lambda_{\text{in}})} \cdot \frac{\lambda_{\text{out}}}{\lambda_{\text{in}}} \quad (1)$$

143 where $P_{\text{in}}(\lambda_{\text{in}})$ is the incident power (assumed to be
144 Lambertian) at wavelength λ_{in} and $P_{\text{out}}(\lambda_{\text{out}}, \Omega)$ is the radiant
145 power emitted into the solid angle Ω with wavelength λ_{out} .
146 **Equation 1** gives the ratio of the number of photons emitted
147 within the solid angle Ω_0 to the number of incident photons.
148 Note that the integrated F over full space ($\Omega_0 = 4\pi$) is equal to
149 1 for a luminescent layer that absorbs 100% of the incident light
150 and emits with unity fluorescence quantum efficiency (QY).
151 Therefore, the nanoantenna array will demonstrate optical
152 etendue reduction if there exist a value of Ω_0 for which $F > 1$. It
153 is desirable for an optical detector device to achieve $F \gg 1$ by
154 reemitting photons without loss in a small solid angle $\Omega_0 \rightarrow 0$.
155 The emitted light can then be focused into a small spot with an
156 area inversely proportional to Ω_0 using conventional optics.
157

A first step to achieve $F > 1$ is to maximize the absorption
158 efficiency of the luminescent detector. Starting with a bare dye
159

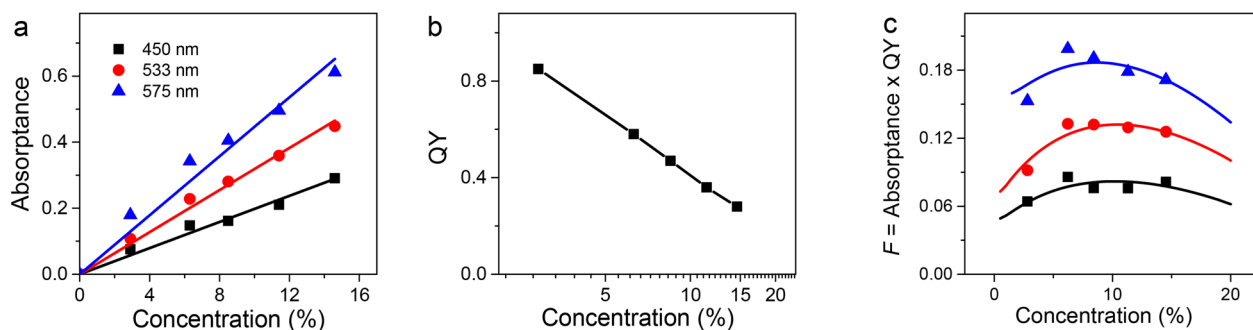


Figure 2. (a) Absorbance of a 700 nm thick polymer layer with Lumogen dye molecules as a function of the dye concentration in weight percent measured at different wavelengths: 450 nm (blue triangles), 533 nm (red circles), and 575 nm (black squares). (b) Fluorescence quantum yield (QY) of the dye layer as a function of concentration. (c) Figure of merit (F) of the dye layer as a function of concentration calculated from the absorbance and QY measurements of (a) and (b). The solid lines and curves are guides to the eye.

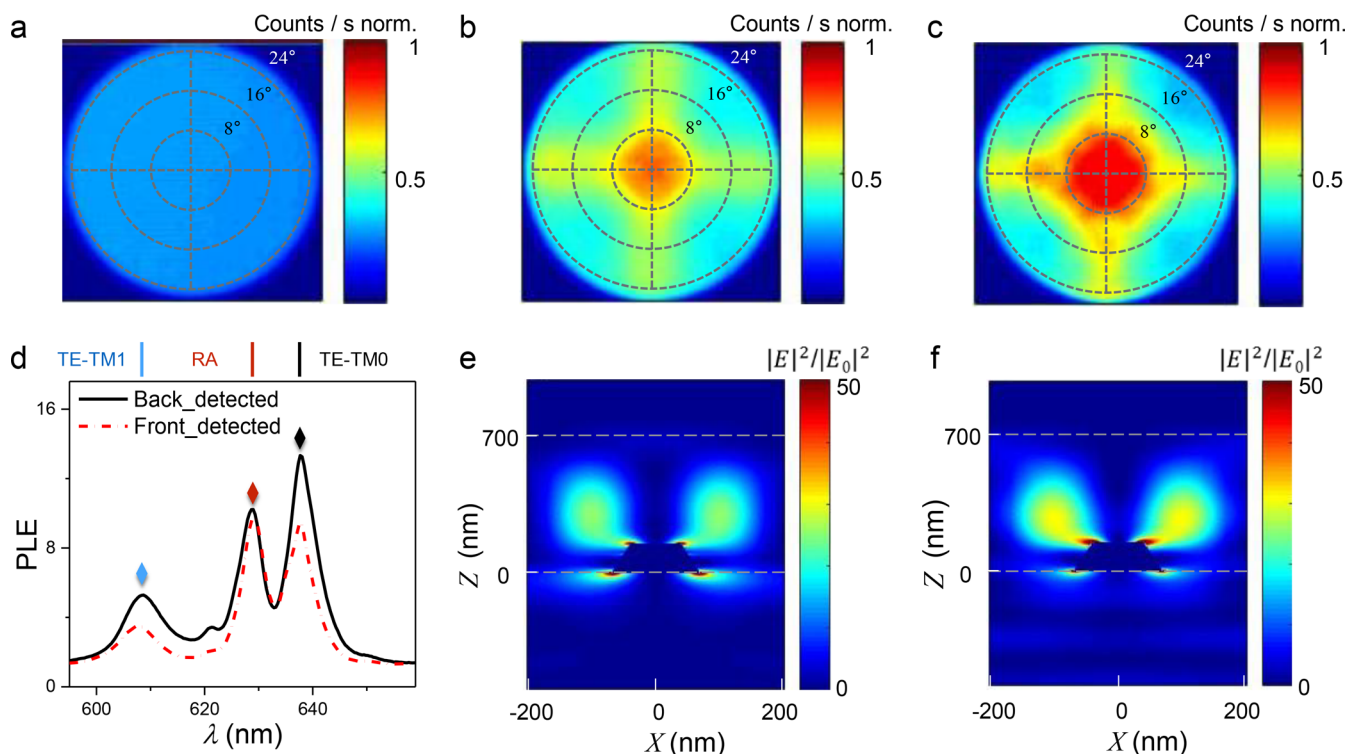


Figure 3. (a) Emission intensity of a polymer layer with Lumogen dye molecules, (b) the dye layer on a nanoparticle array detected from the front side of the array, and (c) the dye layer on the nanoparticle array detected from the back side of the array, as a function of emission angle. The three measurements have been done under the same experimental conditions and are normalized to the same value. The maximum emission angle in the measurements is limited to 26° by the numerical aperture of the objective lens ($NA = 0.45$). (d) Photoluminescence enhancement (PLE), defined as the emission from the nanoparticle array normalized by the emission of the bare dye layer, as a function of the wavelength and measured in the direction perpendicular to the sample surface. The black solid and red dash-dotted curves correspond to the back and front detected intensity enhancements, respectively. The three peaks from right to left correspond to the zero-order quasi-guided modes ($TE-TM_0$), the degenerate ($\pm 1, 0$) and ($0, \pm 1$) Rayleigh anomalies (RAs), and the first-order quasi-guided modes ($TE-TM_1$). Simulated spatial distribution of the near-field intensity enhancement in a unit cell of the nanoparticle array. The simulations are performed for a plane wave incident with a wavelength of 638 nm (corresponding to the $TE-TM_0$ modes in (d)) incident normal to the array from the front (e) and back (f) side.

160 layer where the dye molecules are isotropically dispersed in the
 161 polymer matrix and the emission is Lambertian, the absorption
 162 of the excitation beam can be maximized by increasing the
 163 concentration of the molecules or the layer thickness. However,
 164 in order to increase the emission in the forward direction with
 165 the nanoparticle array, as shown later, the layer thickness needs
 166 to be kept below $1 \mu\text{m}$.²⁵ Increasing the molecular
 167 concentration also leads to concentration quenching of the
 168 emission and the reduction of the QY. This reduces the
 169 efficiency of the luminescence process quantified by $F(4\pi)$,

170 which is given by to the product of the absolute absorption and
 171 the quantum yield (QY) of the bare dye film. Therefore, F for
 172 thin molecular layers are typically much smaller than one.

173 **Figure 2** displays measurements of the absorbance (A), QY,
 174 and integrated F for various dye layers with the same thickness
 175 of 700 nm, containing different molecular concentrations and
 176 for different excitation wavelengths ($\lambda_{\text{in}} = 450, 533, \text{ and } 575$
 177 nm). The absorbance was determined from the conservation
 178 of energy, that is, $A = 1 - T - R$, where T is the transmittance
 179 of the normal incident beam through the dye film and R is the

180 reflectance. The absorption of the dye molecules at each
 181 wavelength increases linearly as a function of the dye
 182 concentration. At $\lambda_{in} = 575$ nm, the dye molecules present
 183 the highest absorbance as it is shown in Figure 2a. The QY of
 184 the same layers was measured with an integrating sphere and it
 185 is shown in Figure 2b.²⁶ The QY of the dye is reduced by
 186 increasing concentration, which is mainly associated with the
 187 aforementioned emission quenching due to the increase of the
 188 nonradiative energy transfer between neighboring dye mole-
 189 cules.^{27,28} Consequently, a maximum value of the integrated F
 190 of 0.2 for the bare dye film is obtained for a concentration of
 191 ~ 8.5 wt % and by exciting the layer at $\lambda_{in} = 575$ nm (see Figure
 192 2c). In what follows, we show that the plasmonic nanoantenna
 193 array can improve F by enhancing the directional emission of
 194 the dye layer.

195 ■ DIRECTIONAL EMISSION OF NANOANTENNA 196 ARRAYS

197 The emission directivity of the dye layer with and without the
 198 nanoantenna array was characterized with a confocal Fourier
 199 setup schematically represented in Figure S3 and described in
 200 the Supporting Information. The emission from the sample was
 201 collected by a 20 \times microscope objective with a numerical
 202 aperture (NA) of 0.45. The emission intensity of the sample as
 203 a function of the angle was recorded in the back focal plane of
 204 the objective with a Fourier lens. Figure 3a–c show the Fourier
 205 images of the emission from the bare dye layer, the emission of
 206 the dye layer on top of the nanoantenna array detected from
 207 the front side, that is, the particle array side facing the objective
 208 lens, and the back detected emission of the dye layer on top of
 209 the nanoantennas, that is, the substrate side of the sample
 210 facing the objective lens, respectively. Note that these
 211 measurements were performed under the same conditions
 212 and normalized to the same value to facilitate a direct
 213 comparison. The emission from the bare dye film displays a
 214 nearly isotropic distribution within the maximum angle
 215 measured ($\theta_{em} = 26^\circ$), corresponding to its Lambertian
 216 properties. The emission from the dye layer on top of the
 217 nanoparticle array is predominantly confined in a small solid
 218 angle. This pronounced beaming effect is due to the emission
 219 decay into the SLRs and quasi-guided modes supported by the
 220 dye layer on the particle array and the subsequent outcoupling
 221 of the emission to free space in a defined direction.^{29–31}

222 Interestingly, the beaming effect detected from the back side of
 223 the particle array is more pronounced than the one observed
 224 from the front side. As we will show later, this is mainly due to
 225 the different fractional density of optical states (FLDOS) in the
 226 two directions because of the tapered shape of the nano-
 227 particles.

228 The photoluminescence enhancement (PLE) spectra,
 229 defined as the PL of the dye layer on top of the particle
 230 array normalized by the PL of the same layer on top of the flat
 231 substrate and recorded in the normal direction ($\theta_{em} = 0^\circ$) are
 232 presented in Figure 3d. To distinguish the different peaks in the
 233 spectra, we have determined the angular dispersion of the
 234 particle array sample by measuring the extinction (see Figure
 235 S1). The dispersion curves are well described by the grating and
 236 planar waveguide phase matching equations and neglecting the
 237 coupling between the different modes. Based on these
 238 extinction measurements, we can assign the three main peaks
 239 of the PLE spectra in Figure 3d to the zero-order quasi-
 240 guided modes (TE–TM₀) coupled into free space through the
 241 lattice diffraction orders, the Rayleigh anomalies (RAs), and the

242 first-order quasi-guided modes (TE–TM₁). Due to the small
 243 energy differences between TE and TM modes,³¹ a single peak,
 244 instead of two, is observed in the PLE spectra. The solid black
 245 curve in Figure 3d corresponds to the emission detected from
 246 the backside of the particle array sample. This emission shows a
 247 14-fold, 10-fold, and 5.8-fold PLE at the TE–TM₁, RAs, and
 248 TE–TM₀ frequencies, respectively. The dash-dotted red curve
 249 in the same figure corresponds to the emission detected from
 250 the front side of sample and shows an overall lower
 251 enhancement. The integrated directional enhancement over
 252 the emission spectra detected from the back side is 1.2 \times higher
 253 than the one measured from the front side.

254 To gain more physical insight in the asymmetry of the
 255 detected emission intensity, we have simulated the electric field
 256 (E) intensity profile at the position of the dye layer when
 257 illuminated by a plane wave from both sides using a commercial
 258 finite-difference in time-domain (FDTD) solver. Bloch periodic
 259 boundary conditions were used on the boundaries of the unit
 260 cell of the array and perfectly matched absorbing layers were
 261 used on the vertical boundaries of the simulation volume. The
 262 optical constants of the Al used in the simulation was obtained
 263 from the literature³² and fitted using the Drude model. The
 264 incident wave in the simulations was a broadband pulse
 265 incident along the normal direction. These simulations
 266 represent the FLDOS of the system and are related to the
 267 experiments by reciprocity, that is, a local source will emit
 268 preferentially in a given direction when the local field at the
 269 position of the source for a plane wave incident from this
 270 direction is the highest.³³ As an example for the TE–TM₁
 271 mode, Figure 3e shows the E -field intensity in the xoz plane
 272 crossing the center of a nanoparticle in a unit cell of the array
 273 when illuminated by a plane wave incident from the front side
 274 of the sample along the normal direction. The color scale
 275 represents the field intensity normalized by the incident field
 276 intensity. This simulation can be compared to the emission
 277 shown in Figure 3b. Similarly, in Figure 3f the E -field intensity
 278 is calculated for illumination by a plane wave incident from the
 279 back side of the sample to compare with the emission shown in
 280 Figure 3c. The results of Figures 3e,f show that the E -field
 281 intensity for the illumination from the back and front side have
 282 different enhancement and slightly different shape, which leads
 283 to the detected asymmetry in the emission intensity from the
 284 array.

285 After the optimization of the dye concentration and the
 286 description of the asymmetric beaming effect of the nano-
 287 pyramid array, we set out to measure the $F(\Omega_0)$ of the
 288 nanoparticle array. Experimentally, the emitted power was
 289 measured in two steps due to the broad emission spectrum of
 290 the dye layer (from 560 to 780 nm): First, the integrated power
 291 over the solid angle Ω_0 of the emitted photon flux passing
 292 through a 620 nm band-pass filter with a bandwidth of 10 nm
 293 was measured with a calibrated power meter, $P_{out}(620)$.
 294 Second, the emission spectrum over the same Ω_0 was recorded
 295 with a fiber-coupled spectrometer with and without the band-
 296 pass filter. To ensure that the spectrum was measured correctly,
 297 we have calibrated its photon counts response in the
 298 wavelength range from 400 to 800 nm with a certified halogen
 299 lamp. Here, we call the ratio of the photon counts measured by
 300 the spectrometer with and without band-pass filter as $\mathcal{R}(620)$.
 301 The power of the emitted photon flux without the band-pass
 302 filter is given by

$$P_{out} = P_{out}(620) \cdot \mathcal{R}(620) \quad (2) \quad 303$$

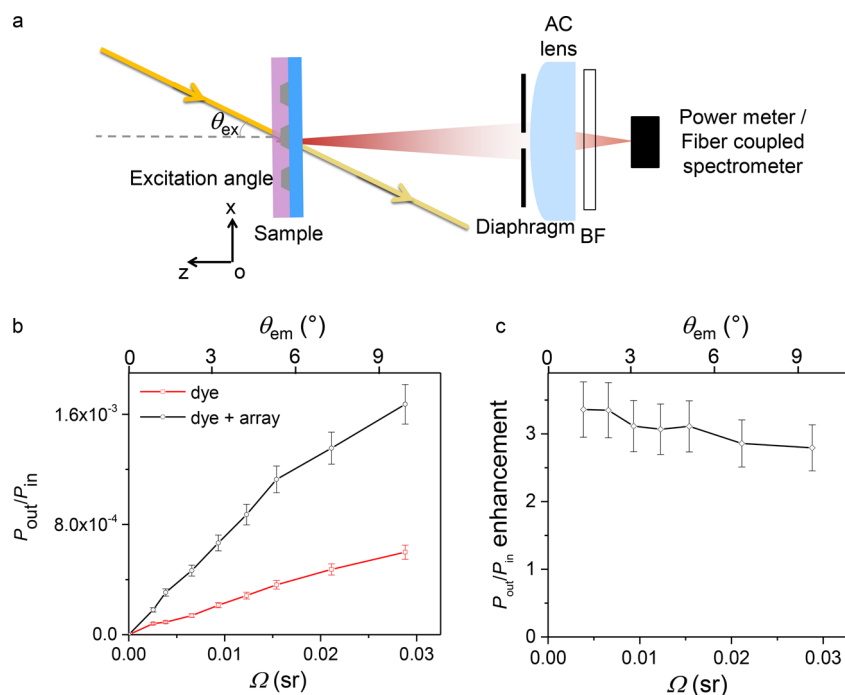


Figure 4. (a) Schematic representation of the optical setup used for the characterization of the figure of merit of luminescent nanoparticle arrays. A laser beam excites the sample at an angle θ_{ex} with respect to the sample normal. The emitted photon flux passes through a diaphragm, an achromatic (AC) lens, a band-pass filter (BF) and is detected by a silicon power meter or fiber coupled spectrometer. The distance between the sample and the diaphragm is fixed to 50 mm. (b) Ratio of the measured emitted power (P_{out}) and the excitation laser beam power (P_{in}) as a function of the collection solid angle (or the elevation angle θ_{em}) in the case of bare dye layer (red squares) and the nanoparticle array with the dye layer on top (black circles). (c) Emission power enhancement of the dye layer due to the nanoparticle array as a function of the collection solid angle.

Figure 4a illustrates a schematic of the setup for the measurements of F as a function of Ω_0 . The sample was illuminated by the laser beam incident at angle θ_{ex} . The emitted light from the sample within Ω_0 is collected by an achromatic lens. The solid angle can be tuned with a variable diameter diaphragm. The distance between the sample and the diaphragm was kept constant at $l = 50$ mm. The irradiance of the excitation beam and the emission signal from the sample passing through the 620 nm band-pass filter (fwhm = 10 nm) was recorded by a silicon power meter. The spectra of the emitted light were taken with the fiber-coupled spectrometer. Compared with the distance between the nanoparticle array and the optical diaphragm defining Ω_0 , the small-excited area on the sample (~ 1 mm²) can be approximated by a point-like light source. Hence, the solid angle of the emitted photon flux passing through the diaphragm and collected by the achromatic lens can be approximated to

$$\Omega_0 \approx \pi \left[\frac{D}{2l} \right]^2 \quad (3)$$

where D is the diameter of the diaphragm. The values of $\int_0^{\Omega_0} P_{\text{out}}(\lambda_{\text{out}}, \Omega) \cdot d\Omega / P_{\text{in}}(\lambda_{\text{in}})$ (for simplicity, named as $P_{\text{out}}/P_{\text{in}}$) as a function of Ω_0 for small solid angles in the forward direction are presented in Figure 4b. The significantly lower P_{out} compared to P_{in} is mainly due to the small collection angle in these experiments and not to losses in the array of metallic nanoparticles. For instance, the power reduction is 50 dB when the emitted light is collected within $\Omega_0 = 0.01$ sr. However, the value of $P_{\text{out}}/P_{\text{in}}$ increases by enlarging the collection solid angle (see Figure 4b). The ratio of $P_{\text{out}}/P_{\text{in}}$ measured with the particle array to the one measured onto the bare dye layer is displayed in Figure 4c as $P_{\text{out}}/P_{\text{in}}$ enhancement.

The maximum $P_{\text{out}}/P_{\text{in}}$ enhancement factor in the normal direction is ~ 3.4 . The enhancement factor decreases for larger collection solid angles because of the strong beaming in small solid angles provided by the nanoparticle array (shown in Figure 3c). In addition, and as expected from eq 1, the F of the bare dye layer is enhanced by the particle array by a factor of ~ 3 for $\Omega_0 = 0.015$ sr.

Figure 5a,b show the results of $F(\Omega_{0,\text{max}})$ measured with the excitation laser beam at $\lambda_{\text{in}} = 533$ and 575 nm, respectively, and $\Omega_{0,\text{max}} = 6.3 \times 10^{-3}$ sr, that is, the solid angle of maximum enhancement of the emission on the forward direction. Note that in such regime of small solid angles, F is independent of Ω_0 , as shown by the linear behavior on Figure 4b. With these measurements, we have also investigated the directional excitation dependence of the sample by varying the elevation angle of the incident angle of the laser beam with respect to surface normal and recording F at the beam perpendicular to the surface for the two sample sides. Comparing Figure 5a,b, F for $\lambda_{\text{in}} = 575$ nm is always larger than for $\lambda_{\text{in}} = 533$ nm, in accordance to the higher absorption of the dye molecules at that wavelength. The triangle in Figure 5a,b correspond to F measured from the back-side, while the circles are the measurements from the front-side. We verify in these figures that F for the bare dye film is insensitive to the angle of incidence and to the detection configuration. However, for the particle array F presents a small dependence on the angle of incidence, which can be attributed to the angular dependent scattering of the excitation beam with the nanoparticle array. The dependence of F with excitation angle (see the blue triangles and the red circles in Figure 5a,b) is smaller than $\sim 20\%$ demonstrating a good omnidirectionality of the absorption over a large field of view. The value of F measured

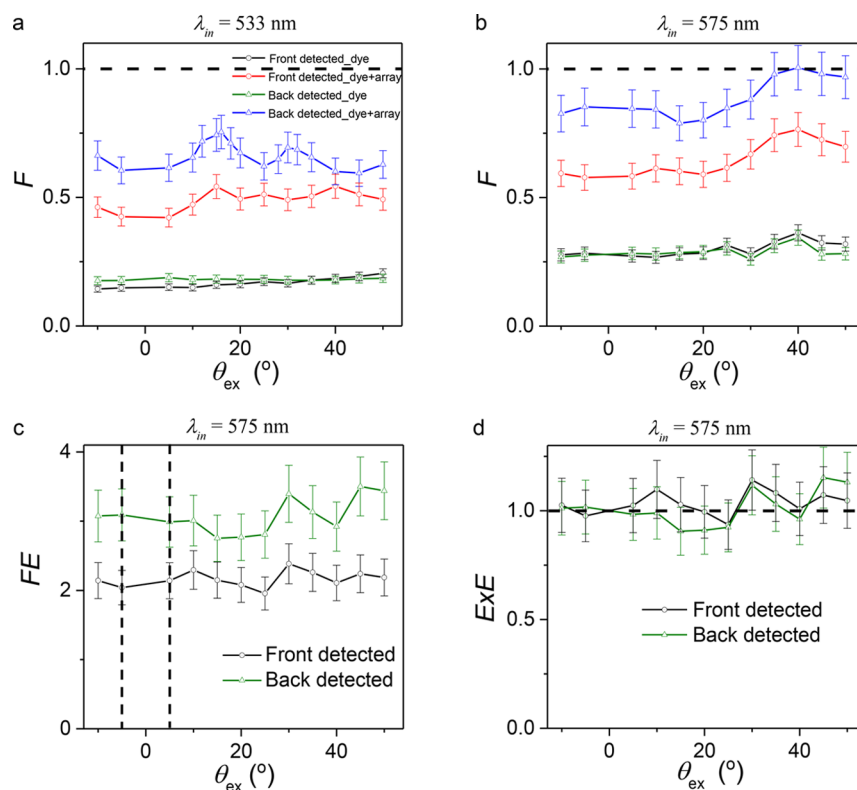


Figure 5. Emission figure of merit as a function of the excitation angle (θ_{ex}) for a pump laser beam of $\lambda_{\text{in}} = 533$ nm (a) and $\lambda_{\text{in}} = 575$ nm (b). The black and red open circles denote F of the bare dye layer and dye layer on the particle array, respectively, and detected from the front side. The green and blue triangles represent F of the bare dye layer and dye layer on the particle array, respectively, and detected from the back side. (c) the F enhancement (FE) obtained from (b) by dividing the F of dye layer on the particle array by the F of the bare dye layer. The FE as a function of θ , normalized by the averaged value of FE measured in the range $-5^\circ \leq \theta \leq 5^\circ$ (indicated by the vertical dashed lines in (c)), result in the excitation enhancement (ExE) shown in (d). In (c) and (d), the solid black circles and green triangles denote the results for the front and back detection configuration, respectively.

366 from the back side of the sample is higher than the one
 367 obtained from the front side (shown in Figure S4a), which is
 368 consistent with the previously described asymmetric beaming
 369 effect in Figure 3. F is enhanced by the particle array by ~ 3
 370 times when detected from the back side of the sample and ~ 2
 371 times from the front side (shown in Figure 5c). In particular, F
 372 can be near unity when the emission is detected from the back
 373 side of the particle array and the 575 nm laser beam excites the
 374 sample with the incident angle of 40° . This near unity F
 375 indicates that the thin and nonperfectly absorbing dye layer
 376 with the nanoparticle array sample has the same performance in
 377 emission and in a small solid angle as an ideal Lambertian
 378 luminescent layer with full absorption and unity fluorescence
 379 QY.

380 To understand the enhancement of F by the nanoparticle
 381 array, we have analyzed its optical resonances at $\lambda_{\text{in}} = 533$ and
 382 575 nm by measuring the extinction spectra of the sample as a
 383 function of the angle of incidence (θ , ϕ), where θ is the
 384 elevation angle and ϕ azimuthal axis measured from one of the
 385 principle axis of the square lattice. Figure S1c,d in the
 386 Supporting Information show these measurements as a
 387 function of θ and for $\phi = 0^\circ, 15^\circ, 30^\circ$, and 45° . The extinction
 388 as a function of θ at $\lambda_{\text{in}} = 575$ nm shows broad peaks that can
 389 be partially attributed to LSPRs in the individual nanoparticles.
 390 In the angle range $-5^\circ \leq \theta \leq 5^\circ$ there are no scattering
 391 resonances excited, which means that the excitation enhance-
 392 ment (ExE) for these incident angles can be neglected.
 393 Consequently, the enhancement of F , which we call FE, at

other angles of incidence can be normalized by the averaged 394
 results in this range (indicated by the vertical dashed lines in 395
 Figure 5c), leading to the ExE assisted by the LSPRs at the 396
 excitation wavelength of 575 nm. This ExE is displayed in 397
 Figure 5d, where it can be appreciated that the ExE fluctuates 398
 around 1. Additionally, the ExE is insensitive to the detection 399
 configuration as illustrated by the triangles and circles shown in 400
 Figure S4b. This is an expected result due to the small mode 401
 volume of LSPRs, which only efficiently enhances the 402
 absorption of the small fraction of dye molecules distributed 403
 at the vicinity of the nanoparticles. The FE could also have its 404
 origin in the emission enhancement due to an enhanced 405
 radiative decay rate of the dye molecules assisted by the higher 406
 local density of optical states. However, the fluorescence 407
 lifetime of the dye layer on the particle array is only slightly 408
 reduced (see Figure S2).²³ Therefore, we conclude that the 409
 substantial enhancement of F is mainly due to the asymmetric 410
 beaming effect of the tapered nanopillar.³³ 411

CONCLUSION

412
 In summary, we have demonstrated the potential application of 413
 arrays of metallic nanoparticles to act as etendue reducers and 414
 thereby enhance the response of optical detectors for free-space 415
 optical communication. In particular, we have shown that a 416
 luminescent layer on top of a periodic array of Al nanoparticles 417
 has a strong beamed emission in a solid angle in the forward 418
 direction. This beamed emission can be used to improve the 419
 detected signal by small field of view photodetectors. Using this 420

421 system, we achieve an emission figure of merit close to unity
422 using a thin layer of nonperfectly absorbing dye molecules,
423 which is equivalent to the figure of merit of a perfectly
424 absorbing layer with a quantum efficiency of 100%. In addition,
425 this figure of merit is almost independent of the angle of
426 incidence, which will enable to suppress complex pointing and
427 tracking systems for optical communication.³ Further improve-
428 ment of the beamed emission can be achieved by replacing the
429 layer of dye by a material with a higher absorption efficiency
430 and high quantum yield. Potential candidates are atomic-
431 monolayers of 2D semiconductors,^{34–36} inorganic perov-
432 skites,³⁷ and aggregation induced emission crystals.³⁸ A thinner
433 layer of these materials with higher absorption efficiency will
434 improve the beaming of the emission and, hence, the figure of
435 merit can reach values higher than the maximum value of 1 for
436 bare, perfect emitting layers. This improved beaming can be
437 achieved by positioning the thin layer at the height on the
438 sample of maximum electric field amplitude as has been
439 recently shown in ref 31. Alternative to metallic nanonantennas,
440 also arrays of dielectric Mie resonators could be used,
441 suppressing the losses in the metal. However, the size of the
442 resonators should be larger than the nanoparticles to achieve
443 comparable polarizabilities and scattering efficiencies. In this
444 work, we have not addressed the band-limiting effects induced
445 by the dyes, which can limit the performance if data rates higher
446 than ~2 Gbps are required.³ It has been recently demonstrated
447 that using plasmonic enhancement the radiative rate of the
448 luminescent materials can be boosted over 2 orders of
449 magnitude by leveraging the Purcell effect³⁹ and, therefore,
450 can increase the bandwidth of the optical detectors. In
451 conclusion, plasmonic enhancement provides a promising
452 method to improve the performance of luminescent detectors.

453 ■ ASSOCIATED CONTENT

454 ● Supporting Information

455 The Supporting Information is available free of charge on the
456 ACS Publications website at DOI: 10.1021/acspphoto-
457 nics.8b00298.

458 The optical methods, extinction spectra, photolumines-
459 cence lifetime, and the comparison of the enhancement
460 factors (PDF).

461 ■ AUTHOR INFORMATION

462 Corresponding Authors

463 *E-mail: s.wang@diffen.nl.

464 *E-mail: j.gomez.rivas@tue.nl.

465 ORCID

466 Shaojun Wang: 0000-0002-0812-0782

467 Mohammad Ramezani: 0000-0003-2781-0217

468 Jaime Gomez Rivas: 0000-0002-8038-0968

469 Notes

470 The authors declare no competing financial interest.

471 ■ ACKNOWLEDGMENTS

472 We thank M.A. Verschuuren for the fabrication of the
473 nanoparticle array used in this work. This work is part of the
474 research programme of The Netherlands Organisation for
475 Scientific Research (NWO). J.G.R. would also like to
476 acknowledge financial support through a Facebook Academy
477 Award.

■ REFERENCES

- 478 (1) van Sark, W. G. J. H. M.; Barnham, K. W. J.; Slooff, L. H.;
479 Chatten, A. J.; Büchtemann, A.; Meyer, A.; McCormack, S. J.; Koole,
480 R.; Farrell, D. J.; Bose, R.; et al. Luminescent Solar Concentrators - A
481 Review of Recent Results. *Opt. Express* **2008**, *16*, 21773–21792. 482
- (2) Kharzheev, Y. N. Scintillation Counters in Modern High-Energy
483 Physics Experiments (Review). *Phys. Part. Nucl.* **2015**, *46*, 678–728. 484
- (3) Peyronel, T.; Quirk, K. J.; Wang, S. C.; Tiecke, T. G.
485 Luminescent Detector for Free-Space Optical Communication. *Optica*
486 **2016**, *3*, 787–792. 487
- (4) Curto, A. G.; Volpe, G.; Taminiau, T. H.; Quidant, R.; Hulst, N.
488 F. van. Unidirectional Emission of a Quantum Dot Coupled to a
489 Nanoantenna. *Science* **2010**, *329*, 930–933. 490
- (5) Tsakmakidis, K. L.; Boyd, R. W.; Yablonovitch, E.; Zhang, X.
491 Large Spontaneous-Emission Enhancements in Metallic Nanostruc-
492 tures: Towards LEDs Faster than Lasers. *Opt. Express* **2016**, *24*,
493 17916–17927. 494
- (6) Mühlshlegel, P.; Eisler, H.-J.; Martin, O. J. F.; Hecht, B.; Pohl, D.
495 W. Resonant Optical Antennas. *Science* **2005**, *308*, 1607–1609. 496
- (7) Vecchi, G.; Giannini, V.; Gómez Rivas, J. Shaping the Fluorescent
497 Emission by Lattice Resonances in Plasmonic Crystals of Nano-
498 antennas. *Phys. Rev. Lett.* **2009**, *102*, 146807. 499
- (8) Steele, J. M.; Gagnidze, I.; Wiele, S. M. Efficient Extraction of
500 Fluorescence Emission Utilizing Multiple Surface Plasmon Modes
501 from Gold Wire Gratings. *Plasmonics* **2010**, *5*, 319–324. 502
- (9) Pellegrini, G.; Mattei, G.; Mazzoldi, P. Nanoantenna Arrays for
503 Large-Area Emission Enhancement. *J. Phys. Chem. C* **2011**, *115*,
504 24662–24665. 505
- (10) Zhou, W.; Odom, T. W. Tunable Subradiant Lattice Plasmons
506 by out-of-Plane Dipolar Interactions. *Nat. Nanotechnol.* **2011**, *6*, 423–
507 427. 508
- (11) Teperik, T.; Degiron, A. Superradiant Optical Emitters Coupled
509 to an Array of Nanosize Metallic Antennas. *Phys. Rev. Lett.* **2012**, *108*,
510 147401. 511
- (12) Saito, H.; Yamamoto, N. Control of Light Emission by a
512 Plasmonic Crystal Cavity. *Nano Lett.* **2015**, *15*, 5764–5769. 513
- (13) Zakharko, Y.; Graf, A.; Schiessl, S. P.; Hahnlein, B.; Pezoldt, J.;
514 Gather, M. C.; Zaumseil, J. Broadband Tunable, Polarization-Selective
515 and Directional Emission of (6,5) Carbon Nanotubes Coupled to
516 Plasmonic Crystals. *Nano Lett.* **2016**, *16*, 3278–3284. 517
- (14) Zakharko, Y.; Held, M.; Graf, A.; Rodlmeier, T.; Eckstein, R.;
518 Hernandez-Sosa, G.; Hahnlein, B.; Pezoldt, J.; Zaumseil, J. Surface
519 Lattice Resonances for Enhanced and Directional Electroluminescence
520 at High Current Densities. *ACS Photonics* **2016**, *3*, 2225–2230. 521
- (15) Laux, F.; Bonod, N.; Gérard, D. Single Emitter Fluorescence
522 Enhancement with Surface Lattice Resonances. *J. Phys. Chem. C* **2017**,
523 *121*, 13280–13289. 524
- (16) Guo, R.; Derom, S.; Väkeväinen, A. I.; van Dijk-Moes, R. J. A.;
525 Liljeroth, P.; Vanmaekelbergh, D.; Törmä, P. Controlling Quantum
526 Dot Emission by Plasmonic Nanoarrays. *Opt. Express* **2015**, *23*,
527 28206–28215. 528
- (17) Stehr, J.; Crewett, J.; Schindler, F.; Sperling, R.; von Plessen, G.;
529 Lemmer, U.; Lupton, J. M.; Klar, T. a.; Feldmann, J.; Holleitner, a. W.;
530 et al. A Low Threshold Polymer Laser Based on Metallic Nanoparticle
531 Gratings. *Adv. Mater.* **2003**, *15*, 1726–1729. 532
- (18) Zhou, W.; Dridi, M.; Suh, J. Y.; Kim, C. H.; Co, D. T.;
533 Wasielewski, M. R.; Schatz, G. C.; Odom, T. W. Lasing Action in
534 Strongly Coupled Plasmonic Nanocavity Arrays. *Nat. Nanotechnol.*
535 **2013**, *8*, 506–511. 536
- (19) Schokker, A. H.; Koenderink, A. F. Lasing at the Band Edges of
537 Plasmonic Lattices. *Phys. Rev. B: Condens. Matter Mater. Phys.* **2014**, *90*,
538 155452. 539
- (20) Garcia De Abajo, F. J. Colloquium: Light Scattering by Particle
540 and Hole Arrays. *Rev. Mod. Phys.* **2007**, *79*, 1267–1290. 541
- (21) Christ, A.; Tikhodeev, S. G.; Gippius, N. A.; Kuhl, J.; Giessen,
542 H. Waveguide-Plasmon Polaritons: Strong Coupling of Photonic and
543 Electronic Resonances in a Metallic Photonic Crystal Slab. *Phys. Rev.*
544 *Let.* **2003**, *91*, 183901. 545

- 546 (22) Murai, S.; Verschuuren, M. A.; Lozano, G.; Pirruccio, G.;
547 Rodriguez, S. R. K.; Rivas, J. G. Hybrid Plasmonic-Photonic Modes in
548 Diffractive Arrays of Nanoparticles Coupled to Light-Emitting Optical
549 Waveguides. *Opt. Express* **2013**, *21*, 4250.
- 550 (23) Lozano, G.; Louwers, D. J.; Rodríguez, S. R.; Murai, S.; Jansen,
551 O. T.; Verschuuren, M. A.; Gómez Rivas, J. Plasmonics for Solid-State
552 Lighting: Enhanced Excitation and Directional Emission of Highly
553 Efficient Light Sources. *Light: Sci. Appl.* **2013**, *2*, e66.
- 554 (24) Verschuuren, M. Substrate Conformal Imprint Lithography for
555 Nanophotonics. *Ph.D. thesis*, Univ. Amsterdam, 2009.
- 556 (25) Nikitin, A.; Remezani, M.; Rivas, J. G. Luminescent
557 Metamaterials for Solid State Lighting. *ECS J. Solid State Sci. Technol.*
558 **2016**, *5*, R3164–R3169.
- 559 (26) de Mello, J. C.; Felix Wittmann, H.; Friend, R. H. An Improved
560 Experimental Determination of External Photoluminescence Quantum
561 Efficiency. *Adv. Mater.* **1997**, *9*, 230–232.
- 562 (27) Lakowicz, J. R. *Principles of Fluorescence Spectroscopy*, 3rd ed.;
563 Springer, 2006.
- 564 (28) Wang, S.; Chervy, T.; George, J.; Hutchison, J. A.; Genet, C.;
565 Ebbesen, T. W. Quantum Yield of Polariton Emission from Hybrid
566 Light-Matter States. *J. Phys. Chem. Lett.* **2014**, *5*, 1433–1439.
- 567 (29) Lozano, G.; Grzela, G.; Verschuuren, M. A.; Ramezani, M.;
568 Rivas, J. G. Tailor-Made Directional Emission in Nanoimprinted
569 Plasmonic-Based Light-Emitting Devices. *Nanoscale* **2014**, *6*, 9223–
570 9229.
- 571 (30) Guo, K.; Lozano, G.; Verschuuren, M. A.; Gómez Rivas, J.
572 Control of the External Photoluminescent Quantum Yield of Emitters
573 Coupled to Nanoantenna Phased Arrays. *J. Appl. Phys.* **2015**, *118*,
574 73103.
- 575 (31) Ramezani, M.; Lozano, G.; Verschuuren, M. A.; Gómez Rivas, J.
576 Modified Emission of Extended Light Emitting Layers by Selective
577 Coupling to Collective Lattice Resonances. *Phys. Rev. B: Condens.*
578 *Matter Mater. Phys.* **2016**, *94*, 125406.
- 579 (32) Palik, E. D. *Handbook of Optical Constants of Solids*; Academic
580 Press, 1985.
- 581 (33) Rodriguez, S. R. K.; Arango, F. B.; Steinbusch, T. P.;
582 Verschuuren, M. A.; Koenderink, A. F.; Rivas, J. G. Breaking the
583 Symmetry of Forward-Backward Light Emission with Localized and
584 Collective Magnetoelectric Resonances in Arrays of Pyramid-Shaped
585 Aluminum Nanoparticles. *Phys. Rev. Lett.* **2014**, *113*, 247401.
- 586 (34) Amani, M.; Lien, D.; Kiriya, D.; Xiao, J.; Azcatl, A.; Noh, J.;
587 Madhupathy, S. R.; Addou, R.; Kc, S.; Dubey, M.; et al. Near-Unity
588 Photoluminescence Quantum Yield in MoS₂. *Science* **2015**, *350*,
589 1065–1068.
- 590 (35) Kim, H.; Lien, D.-H.; Amani, M.; Ager, J. W.; Javey, A. Highly
591 Stable Near-Unity Photoluminescence Yield in Monolayer MoS₂ by
592 Fluoropolymer Encapsulation and Superacid Treatment. *ACS Nano*
593 **2017**, *11*, 5179–5185.
- 594 (36) Wang, S.; Li, S.; Chervy, T.; Shalabney, A.; Azzini, S.; Orgiu, E.;
595 Hutchison, J. A.; Genet, C.; Samorì, P.; Ebbesen, T. W. Coherent
596 Coupling of WS₂ Monolayers with Metallic Photonic Nanostructures
597 at Room Temperature. *Nano Lett.* **2016**, *16*, 4368–4374.
- 598 (37) Zhang, Q.; Su, R.; Liu, X.; Xing, J.; Sum, T. C.; Xiong, Q. High-
599 Quality Whispering-Gallery-Mode Lasing from Cesium Lead Halide
600 Perovskite Nanoplatelets. *Adv. Funct. Mater.* **2016**, *26*, 6238–6245.
- 601 (38) Duan, Y.; Ju, C.; Yang, G.; Fron, E.; Coutino-Gonzalez, E.;
602 Semin, S.; Fan, C.; Balok, R. S.; Cremers, J.; Tinnemans, P.; et al.
603 Aggregation Induced Enhancement of Linear and Nonlinear Optical
604 Emission from a Hexaphenylene Derivative. *Adv. Funct. Mater.* **2016**,
605 *26*, 8968–8977.
- 606 (39) Traverso, A. J.; Huang, J.; Peyronel, T.; Tiecke, T. G.,
607 Mikkelsen, M. H. Towards a Large, Ultrafast, Detector for Free-Space
608 Optical Communication.